ACS Chemical Neuroscience

Research Article

pubs.acs.org/chemneuro

Lipid Microdomains in Synapse Formation

C. Madwar, G. Gopalakrishnan,* and R. Bruce Lennox*

Department of Chemistry, McGill University, 801 Sherbrooke Street West, Montreal, Quebec H3A 0B8, Canada

Supporting Information

ABSTRACT: Membrane lipid rafts (i.e., cholesterol/sphingolipids domains) exhibit functional roles in both healthy and pathological states of the nervous system. However, due to their highly dynamic nature, it remains a challenge to characterize the fundamental aspects of lipid rafts that are important for specific neuronal processes. An experimental approach is presented here that allows for the interfacing of living neurons with an experimentally accessible model membrane where lipid order in cellular rafts can be reproducibly mimicked. It is demonstrated that coexisting lipid microdomains in model membranes can regulate axonal guidance and establish stable presynaptic contacts when interfaced with neurons in vitro. Experimental evidence is provided where specific functional groups and lateral organizations are favored by neurons in establishing synaptic connections. The model membrane platform presented in this work provides an accessible and direct means to investigate how lipid rafts regulate synapse formation. This experimental platform can similarly be extended to explore a variety of other cellular events where lipid lateral organization is believed to be important.

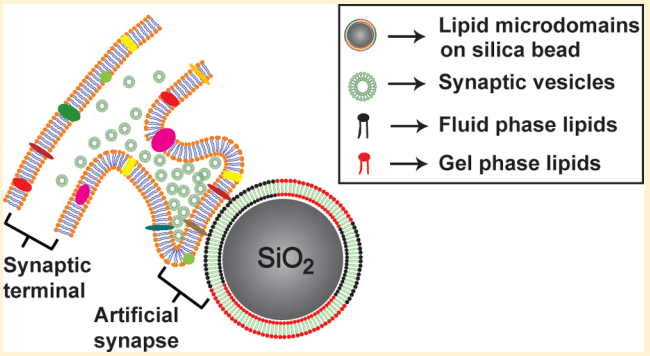

KEYWORDS: *Lipid membranes, supported bilayers, membrane microdomains, lipid rafts, artificial synapses, synaptic vesicles, hippocampal neurons*

Lipid rafts are specialized membrane domains that have been shown to exist in cell plasma membranes.[1,2] They are responsible for a number of cellular processes including regulation of signaling molecules, neuronal outgrowth, axonal guidance, and synaptic transmission.[3−7] Such microdomains consist of both protein and lipid components with an enrichment of sphingolipids and cholesterol resulting in a more ordered lipid bilayer state that exists within the rest of the fluid plasma membrane.[8−10] The dynamic nature of the molecular ordering and packing in these lipid rafts provides modulation of signaling molecules within the membrane and is therefore linked to the excitatory and inhibitory effects of signaling events.[2,11−13] Several reports provide evidence for the involvement of lipid rafts in different neuronal processes, establishing their functional roles in both healthy and pathological states.[14−23] It has also been shown that disruption of membrane rafts can lead to an eventual retraction of neurite outgrowths.[24] A variety of cellular processes essential for neuronal activity and membrane turnover in the brain are thus regulated at lipid rafts and are highly dependent on their organization and dynamics.[20,25] However, the fundamental aspects of lipid rafts that are significant in axonal outgrowth and more importantly, in the initial signaling to establish neuronal activity are still poorly understood. It is therefore of interest to explore the relationship between neuronal activity and lipid rafts using an experimentally accessible and reproducible model system. We demonstrate here the application of a synthetic platform that contains only lipids which display coexisting microdomains. These are shown to regulate axonal guidance and can establish synaptic contacts without any participation of other raft components or postsynaptic elements. Experimental evidence is presented where fluid−gel (L_d−S_o) phase separation is required and one particular fluid coexisting lipid phase is favored by the neurons in establishing synaptic contacts.

We have previously demonstrated the in vitro formation of presynapses on micrometer-sized spherical substrates coated with either a synthetic polypeptide (i.e., poly-D-lysine; PDL)[26,27] or lipid bilayer membranes.[28,29] These reports have shown that the spherical geometry of these substrates is considerably favored for the observation of a functional synaptic response using microscopy techniques. In addition, preliminary evidence suggested that coexisting membrane domains direct lipid membrane-induced synapse formation.[28] However, experimentally establishing the role of lipid phase separation at the initial stages of synapse formation remains a technical challenge.[2,30] This prompted us to generate coexisting lipid microdomains on spherically supported bilayer membranes (SS-BLMs) and use these as an accessible form of lipid "raft-like" environments.[31] In this proof-of-concept study, we demonstrate how extracellular membrane heterogeneity presented on SS-BLMs influences the dynamics of cellular

Received: February 24, 2016
Accepted: March 28, 2016
Published: April 12, 2016

DOI: 10.1021/acschemneuro.6b00058
ACS Chem. Neurosci. 2016, 7, 833−841

microenvironments. This physicochemical model is (i) robust and can withstand cell culture conditions and characterization/imaging procedures,[26−29,31] (ii) interactive with cells at any point in time during the period of cell culture,[26−29,31] (iii) compositionally versatile, displaying structural properties of membranes with minimal components,[28,31] and (iv) of great potential for incorporating functional molecules, such as purified membrane raft components, into the bilayer structure of SS-BLMs.[32,33]

RESULTS AND DISCUSSION

To demonstrate the suitability of our approach in investigating lipid-raft-dependent neuronal outgrowth, SS-BLMs exhibiting coexisting lipid domains were cocultured with primary hippocampal neurons. The interactions between neurons and SS-BLMs can be visualized and examined via fluorescence imaging[31,34−36] using fluorescently tagged lipids (Figure 1).

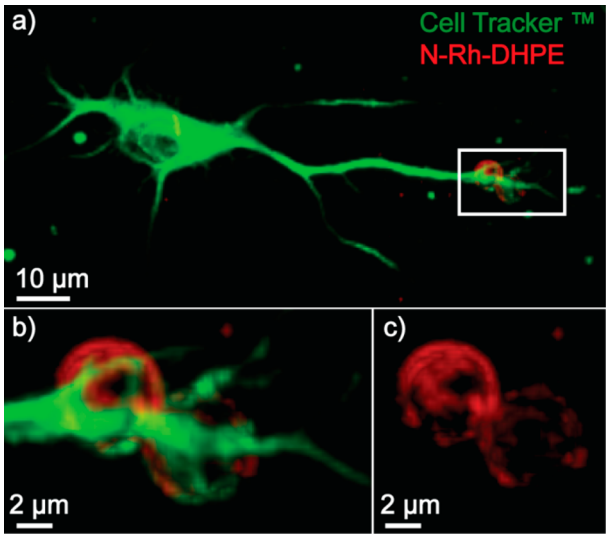

Figure 1. Representative confocal 3D reconstruction images showing the interaction of neurons with lipid microdomains on SS-BLMs displaying a fluid−gel (L_d−S_o) phase coexistence. (a) Assembly of rat hippocampal neurons (DIV 9) around SS-BLMs from DOPC/DPPE/DOTAP (25:50:25). The cells are cocultured with SS-BLMs for 24 h and then labeled with Cell Tracker dye (green). Panel (b) is a magnified view of (a), showing the close interactions between the neuron and the SS-BLMs. Panel (c) is a single channel image of (b), showing the ordered (DPPE-rich) SS-BLM domains labeled using 0.1 mol % N-Rh-DHPE (red areas) and the unlabeled fluid domains (DOPC-rich; dark areas). In this preparation, 5 μm silica beads coated with avidin were used as the spherical solid support and 0.1 mol % DSPE-PEG2000-biotin was used in the lipid mixture for tethering.

These probes are chosen on the basis of their differential ability to partition into different phases.[30] Artificial synapse formation was explored via immunofluorescence methods for visualization of several synaptic proteins in hippocampal neurons.[26−29] These cells were grown for at least 14 days in vitro (DIV) and then cocultured with SS-BLMs of various lipid mixtures for 24 h. Quantification of the fluorescence intensity serves as an indicator of the level of accumulation of synaptic proteins in the vicinity of the SS-BLMs. This allows for exploration of the various chemical and physical parameters of lipid bilayers that trigger a functional synaptic response from the neurons. Moreover, imaging via successive optical sections of the neuron/SS-BLM cocultures (using confocal *Z*-stack imaging) enables the study of the colocalization of synaptic proteins and cytoskeletal networks with different lipid domains. In Figure 1, the imaged neuron was labeled with Cell Tracker dye and the SS-BLMs were labeled with N-Rh-DHPE. This fluorescent lipid preferentially partitions into DPPE-rich ordered lipid domains.[34] Confocal laser scanning microscopy (CLSM) and *Z*-stack imaging were used to examine the assembly of neurons around the different coexisting domains of SS-BLMs in 3D (see Supporting Information Figure S1 for additional representative images of the neuron/SS-BLM interactions).

In our previous studies, SS-BLMs from a particular lipid mixture (DOPC/DPPE/DOTAP (25:50:25)) were shown to induce the formation of presynapses at neuronal contacts.[28] In this study, a statistical analysis comparing the effect of SS-BLMs formed from the above lipid mixture to that of uncoated silica beads was first performed (see Supporting Information Figure S2). In particular, the ability of these SS-BLMs to interact with neurons and induce the formation of presynapses is concluded from the enhanced immunofluorescence of the synaptic vesicle protein synaptophysin, the scaffolding active zone protein bassoon, and the cytoskeletal protein actin in the vicinity of the neuron-bead contact points. A fluorescence quantification analysis compares the fluorescence intensity of these synaptic proteins at the bead surface to that of adjacent areas of the same size (see Supporting Information Figure S3 for details on quantification analysis methods). In this case, a fluorescence intensity ratio (bead site to adjacent area) much greater than unity corresponds to a significant accumulation of the presynaptic vesicles and active zone markers around the SS-BLMs (ratios of synaptophysin are 15.26 ± 2.34 (SS-BLMs) vs 2.24 ± 0.13 (uncoated beads), bassoon 11.65 ± 1.76 (SS-BLMs) vs 1.26 ± 0.22 (uncoated beads), and actin 20.37 ± 2.74 (SS-BLMs) vs 1.76 ± 0.19 (uncoated beads); see Supporting Information Figure S2 and Table S1).

This DOPC/DPPE/DOTAP (25:50:25) ternary lipid mixture bears a net positive charge and exhibits coexisting lipid microdomains at 37 °C (see Supporting Information Figure S4). In order to study which factors favor synapse formation (i.e., headgroup, charge, lipid phase), various mixtures of synthetic phospholipids (Figures 2 and S5−S7) that have different molecular (i.e., different charges and different chemical functional groups) and assembly (i.e., different thermodynamic phases) features were used. In the DOPC/DPPE/DOTAP mixture, the unsaturated DOPC lipids are organized in a loosely packed fluid phase whereas the saturated DPPE lipids are organized in a tightly packed gel phase.[30] Fluorescence intensity analysis shows a significantly low accumulation of the synaptic proteins around homogeneous SS-BLMs in comparison to the above-mentioned DPPE heterogeneous lipid mixtures (Figures 2, 3, and S5). For example, those derived from a lipid mixture containing DOPC/DOPE/DOTAP (25:50:25), where both DOPC and DOPE are intermixed in a homogeneous fluid phase, or those derived from DPPC/DPPE/DOTAP (25:50:25), where both DPPC and DPPE are intermixed in a homogeneous gel phase, show no significant synaptic accumulation at the bead-neuron contacts (Figure 2, panels A and D). The DOPC/DOPE/DOTAP mixture yields fluorescence ratios of synaptophysin 1.06 ± 0.65, bassoon 1.19 ± 0.36 and actin 1.46 ± 0.52 (see Supporting Information Table S1). The DPPC/DPPE/DOTAP mixture yields fluorescence ratios of synaptophysin 1.15 ± 0.31, bassoon 1.51 ± 0.23, and actin 1.65 ± 0.62 (see Supporting Information Table S1). However, it is striking that

DOI: 10.1021/acschemneuro.6b00058
ACS Chem. Neurosci. 2016, 7, 833−841

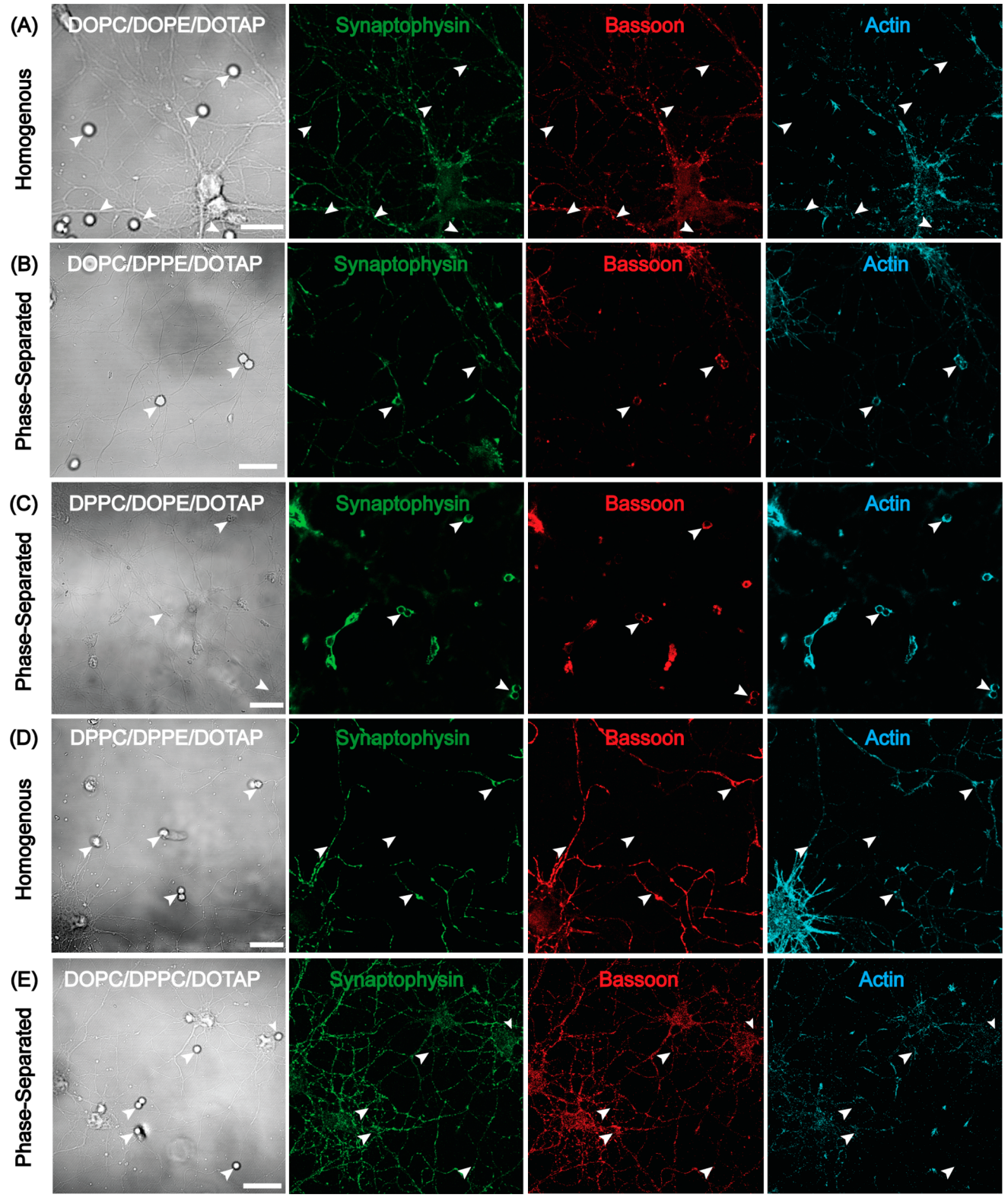

Figure 2. Representative confocal cross section images showing accumulation of presynaptic proteins around SS-BLMs from various lipid mixtures with PC and PE headgroups. In these experiments, SS-BLMs are not labeled. The fluorescence observed around SS-BLMs is due to the immunolabeled presynaptic proteins (i.e., synaptophysin, bassoon, or actin). Rat hippocampal neurons (DIV 22) are incubated for 24 h with SS-BLMs (lipid mixtures are noted on the DIC images; left panel). Neurons are labeled with antibodies specific for synaptophysin (green), bassoon (red), and actin (blue). For each fluorescence image, the corresponding DIC channel is used to locate the beads (white arrows). In this preparation, 5 μm silica beads were coated with avidin and 0.1 mol % DSPE-PEG2000-biotin was used in the lipid mixture for tethering. Scale bars, 20 μm.

when coexisting lipid microdomains formed from a mixture of phosphatidylcholine (PC) lipids (without inclusion of any phosphatidylethanolamine (PE) lipids) were presented to neurons in culture, no presynatic accumulation was observed.

DOI: 10.1021/acschemneuro.6b00058
ACS Chem. Neurosci. 2016, 7, 833−841

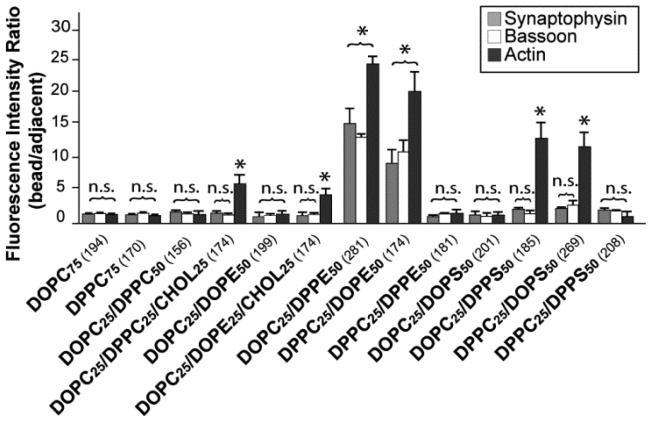

Figure 3. Histograms of fluorescence intensity ratio measurements comparing the accumulation of synaptic proteins (synaptophysin and bassoon) and cytoskeleton proteins (actin) in response to SS-BLMs prepared from various lipid mixtures. Each group was compared to uncoated beads, n.s. is not significant, and $*p < 0.05$ by two-tailed Student's t test after correction for nonequal variance. Values in the histograms are expressed as mean ± standard deviation. The total number of beads analyzed from three independent experiments is given in brackets. In all preparations, hippocampal neurons (DIV 22) were incubated with SS-BLMs for 24 h and then labeled with synaptophysin-, bassoon-, and actin-specific antibodies. In all lipid mixtures, 25 mol % of the positively charged lipid DOTAP (a synthetic lipid that is commonly used as a transfection agent) was added in order to promote the adhesion of the neurons toward SS- BLMs. For all preparations, 5 μm silica beads coated with avidin were used as the solid spherical support and 0.1 mol % DSPE-PEG2000-biotin was used for tethering. Representative confocal images are presented in Figures 2, S6, and S7.

The fluorescence ratios associated with the DOPC/DPPC/DOTAP mixture (Figure 2E) are synaptophysin 1.83 ± 0.21, bassoon 1.26 ± 0.18, and actin 1.43 ± 0.78.

In order to determine if factors other than membrane heterogeneity and PE headgroups are in effect, the role of other membrane lipids (such as phosphatidylserine (PS) and cholesterol) in inducing synapse formation was examined. The fluorescence intensity analysis described earlier was performed on lipid mixtures containing PC and PS lipids. Similarly, the role of cholesterol was studied (representative images are shown in Supporting Information Figures S6 and S7, and fluorescence intensity ratios are summarized in Table S1). Neither case showed any influence on presynapse formation at the lipid–neuron contact points. The quantification of synaptic and cytoskeletal protein levels in the vicinity of the SS-BLMs from the different lipid mixtures (i.e., PC, PE, PS, and cholesterol), presented in either homogeneous or heterogeneous lipid phases, are summarized in Figure 3 (see Supporting Information Table S1 for fluorescence ratio values). In the presence of cholesterol, the resulting SS-BLM lipids intermix, at least on the micrometer scale, in a homogeneous liquid-ordered phase environment, which does not appear to contribute to a significant actin or synaptic proteins accumulation (see Supporting Information Table S1). Additionally, it is interesting to note that in the case of DOPC/DPPS and DPPC/DOPS lipid mixtures, each exhibiting fluid–gel phase separation, there is an elevated actin assembly at the neuron/SS-BLM contact points but no presynaptic protein accumulation. We therefore conclude from the data presented in Figure 3 that lipid phase separation (more specifically, a fluid–gel phase separation) acts as an initial cue for neurons at the axon path-finding stage during artificial synapse formation. However, a combination of fluid–gel lipid phase separation together with headgroup specificity (e.g., PE) in SS-BLMs is the determining factor for transforming these contact sites into functional synaptic points. The question as to why PE headgroups are important in inducing presynaptic assembly requires more thorough investigation but it might be related to their headgroup reactivity or to the membrane curvature PE lipids reportedly induce.

The assembly of synaptic and cytoskeletal proteins in the vicinity of the coexisting lipid phases in the SS-BLM was assessed. A fluorescence colocalization analysis was carried out on dual-color images collected from neuron/SS-BLM cocultures where the cells were immunolabeled for synaptophysin (green) and the SS-BLMs were derived from the synapse inducing lipid mixture DOPC/DPPE/DOTAP (25:50:25) where the ordered lipid domains (DPPE-rich) were labeled in red.

Figure 4, panel (a) shows the merged fluorescence image for the synaptic protein (synaptophysin) and the gel phase domain. In order to evaluate the extent of colocalization, the presence of an overlap in their respective fluorescence intensity profiles is examined. Figure 4, panel (b) shows single fluorescence channels and corresponding fluorescence intensity profiles measured along a line that crosses the bead surface. As seen in

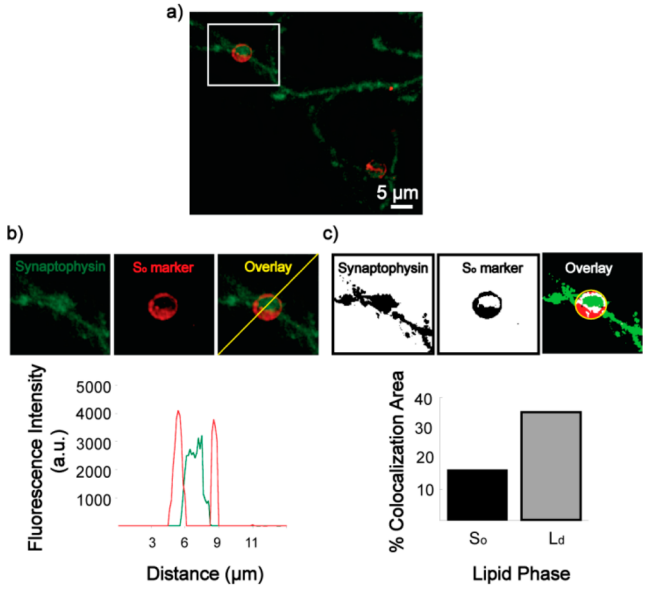

Figure 4. Representative images of a neuron/SS-BLM coculture showing the steps involved in fluorescence colocalization analysis. (a) Confocal 3D reconstruction image of rat hippocampal neurons (DIV 14) incubated for 24 h with SS-BLMs from the ternary mixture DOPC/DPPE/DOTAP (25:50:25) labeled using 0.1 mol % N-Rh-DHPE (red). A close-up on the area highlighted by the white box, which represents the area of the image used for subsequent analysis is shown in (b) as single channel images of the synaptic protein (synaptophysin, green) and ordered lipid phase (S_o, red). Binary images of the corresponding gray scale single channel images are shown in (c). Calculations of fluorescence colocalization from the overlay images by (b) measuring the presence or absence of an overlap of fluorescence intensity profiles across the surface of the SS-BLM (along a defined line, shown in yellow) or (c) measuring the overlap area of fluorescent and nonfluorescent pixels (fluorescent protein pixels with fluorescent (S_o) or nonfluorescent (L_d) lipid pixels, shown in white or green, respectively).

DOI: 10.1021/acschemneuro.6b00058
ACS Chem. Neurosci. 2016, 7, 833–841

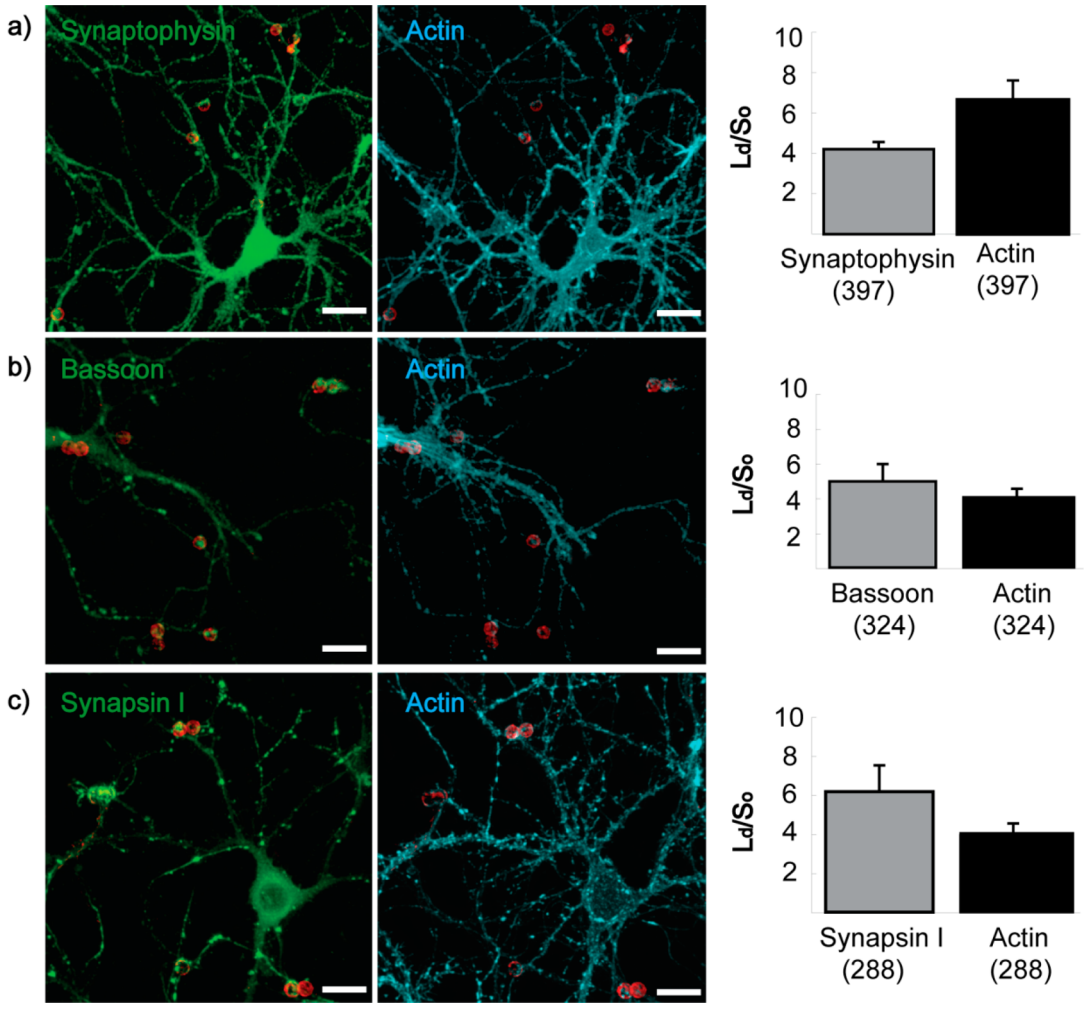

Figure 5. Colocalization of synaptic and cytoskeletal proteins with the lipid phases of SS-BLMs. (a) Representative confocal 3D reconstruction images of rat hippocampal neurons (DIV 14) incubated for 24 h with SS-BLMs of the ternary mixture DOPC/DPPE/DOTAP (25/50/25) displaying fluid−gel (L_d−S_o) phase separation, with the ordered phases (DPPE-rich) labeled using 0.1 mol % N-Rh-DHPE (red). The neurons are labeled for synaptic proteins (green) using antibodies specific for (a) synaptophysin, (b) bassoon, and (c) synapsin I. The F-actin (blue) is labeled using phalloidin. Scale bars, 20 μm. Histograms of the L_d/S_o ratio are shown in the right panels and display the preferential colocalization of the synaptic proteins with the disordered lipid domains (L_d). Percent colocalization data, with either phase, are summarized in Supporting Information Figure S8 and calculated as described in Figure 4. Histograms values are expressed as mean ± standard deviation. The total number of beads analyzed from three independent and identical experiments is given in brackets.

the intensity profile (panel b), the absence of overlap between the green and red channels indicates the absence of colocalization between the synaptic protein synaptophysin (green) and the gel lipid domain (red), suggesting that the synaptic terminals are localized at the (nonlabeled) fluid lipid domain. As outlined in panel (c), the binary images (value of 1 for fluorescent pixels and value of 0 for nonfluorescent pixels) are used in this analysis. In this case, colocalization of the cellular proteins with the lipid phase is indicated by the presence of signal intensity (binary value of 1) from the two fluorescent labels in the same pixel. Within the field of view of the SS-BLM (roughly one-half of the sphere), different areas of pixel overlap (represented by different colors in the overlay image in panel (c)) are defined as (i) white areas, which represent the labeled lipid domains (red) overlapping with the labeled synaptic protein (green), (ii) red areas, which represent the labeled lipid domains (red) not overlapping with the labeled synaptic protein (green), and (iii) green areas, which represent the nonlabeled lipid domains overlapping with the labeled synaptic protein (green). Colocalization areas can be calculated as a fraction of the total bead area, according to the following equations:

$$\%\ \text{colocalization with } L_d = \frac{\text{area of overlap (defined by green area)}}{\text{total area of bead (defined by yellow circle)}} \times 100 \quad (1)$$

$$\%\ \text{colocalization with } S_o = \frac{\text{area of overlap (defined by white area)}}{\text{total area of bead (defined by yellow circle)}} \times 100 \quad (2)$$

This method was applied to analyze the colocalization between the different presynaptic proteins and lipid domains from mixtures containing PE lipids. Colocalization is expressed according to the following equation:

DOI: 10.1021/acschemneuro.6b00058
ACS Chem. Neurosci. 2016, 7, 833−841

$$\text{colocalization ratio } (L_d/S_o) = \frac{\%\text{ colocalization with } L_d}{\%\text{ colocalization with } S_o} \quad (3)$$

The quantitative analysis of colocalization (Figure 5) establishes that there is a significant preference for the accumulation of presynaptic components around fluid phase lipids. This is further confirmed by application of the Pearson correlation coefficient (PCC) methodology,[37] which measures the degree of colocalization between two fluorophores. PCC values generally range between +1 (a perfect colocalization) and −1 (an anticorrelation). The PCC value calculated for the colocalization between the fluorescent proteins and the fluorescent lipid phase (i.e., gel phase) is <0, indicating the absence of protein colocalization with the gel phase (see Supporting Information Figure S9 for a summary of PCC results).

The experiments presented herein demonstrate that SS-BLMs are versatile model system for lipid "raft-like" environment, and when interfaced to neurons in culture, yield new information regarding the initial steps of artificial synapse formation.[38,39] In particular, new insight is developed regarding the chemical and physical properties of lipids that influence the neuronal response to artificial bilayer membranes when cocultured with neurons under physiological conditions. The clustering of presynaptic proteins in the vicinity of SS-BLMs is evident from the presence of a synaptic vesicle protein (synaptophysin), a scaffolding active zone (bassoon), and the cytoskeletal protein (actin). The presence of these three proteins is considered to be a positive neuronal response in synapse formation. Immunofluorescence quantification analysis shows that the interaction of neurons with SS-BLMs results in a significant enrichment of synaptophysin and bassoon at their contact sites. This is observed only when the lipids in SS-BLMs contain phosphatidylethanolamine (PE) headgroups and are in a heterogeneous fluid−gel lipid phase separated state. The small headgroup of PE results a conical shape, which is thought to exert a lateral pressure that modulates the bilayer membrane curvature and helps to stabilize membrane proteins in their optimal conformations.[40] Another feature of PE lipids is the ionizable amine which can also participate in hydrogen bonding.[41] The presence of amino groups in SS-BLMs from other phospholipids such as phosphatidylserine (PS) did not however yield the same results as those observed with PE lipids. This highlights the importance of both (i) the structural details of the lipids (i.e., their functional groups, overall charge, intrinsic shape, curvature-inducing, etc.) and (ii) the cooperative and aggregative properties of the membrane (i.e., its physical organization and the presence of lateral heterogeneity) in lipid-induced artificial synapse formation.

Several studies have shown that a number of signaling molecules responsible for regulating neuronal processes are localized in membrane lipid rafts.[12−14] It has also been demonstrated that nerve growth cones respond to specific substrate surface features,[42] specifically when allowed to grow on substrates with varying stiffness[43] and rheology.[44] Substrates with tunable surface properties have thus been shown to influence neuronal growth and synaptic processes.[45,46] This study, on the other hand, addresses the question of how membrane phase influences neuronal differentiation and outgrowth. The data presented here establish that, in forming functional synapses, neurons prefer the fluid phase within a lipid raft. Since the initial step in artificial synapse formation begins with axonal path-finding, mainly via the actin cytoskeletal networks,[26,47,48] the cytoskeletal networks perhaps perform the "ground work" for the neurons to establish the first attachment points. However, our results clearly demonstrate that an environment of lipid phase separation is not the only requirement, as some of these contact points do not necessarily develop into functional synapses. In order to achieve artificial synapse formation at established contact points, additional parameters such as the headgroup specificity, overall charge, and membrane curvature have to be taken into account.

In summary, fluid lipid phases within a raft-like model platform are found to mediate stable neuronal contact points on membrane substrates. This attachment step being the driving force, additional lipid properties are used to develop these contact points into functional synapses. Raft proteins or postsynaptic components are *not* necessary to establish these active synaptic sites. Given the importance of lipid rafts in cellular processes and cell signaling, the use of SS-BLM-based raft models is a step forward in the experimental study of raft-mediated biological events. Future experiments will involve SS-BLMs of increasing complexity by incorporating proteins and lipid/protein complexes into the bilayer membrane, or by assembling the supported bilayer from native membrane vesicles. The robustness and ease of characterization which SS-BLMs offer will enable the study of the function of key lipids and proteins participating in artificial synapses or other cellular events that involve membrane−membrane interactions.

METHODS

Materials. 1,2-Dioleoyl-*sn*-glycero-3-phosphocholine (DOPC), 1,2-dioleoyl-*sn*-glycero-3-phosphoethanolamine (DOPE), 1,2-dioleoyl-*sn*-glycero-3-phospho-L-serine (sodium salt) (DOPS), 1,2-dioleoyl-3-trimethylammonium propane chloride salt (DOTAP), 1,2-dipalmitoyl-*sn*-glycero-3-phosphocholine (DPPC), 1,2-dipalmitoyl-*sn*-glycero-3-phosphoethanolamine (DPPE), 1,2-dipalmitoyl-*sn*-glycero-3-phospho-L-serine (sodium salt) (DPPS), and 1,2-distearoyl-*sn*-glycero-3-phosphatidylethanolamine-*N*-biotinyl-(polyethylene glycol 2000)] ammonium salt (DSPE-PEG2000-biotin) were purchased from Avanti Polar Lipids (purity > 99%). Lissamine Rhodamine B 1,2-dihexadecanoyl-*sn*-glycero-3-phosphoethanolamine, triethylammonium salt (N-Rh-DHPE), secondary antibodies and Alexa-488/Alexa-647−phalloidin were purchased from Molecular Probes, Invitrogen. Poly-L-lysine hydrobromide was purchased from Sigma. GelTol (aqueous mounting media) was purchased from Shandon Lipshaw Co., Lerner Laboratories. All other cell culture media were purchased from Gibco, Invitrogen.

Formation of SS-BLMs. SS-BLMs were prepared starting with lipid vesicles in the form of small unilamellar vesicles (SUVs). These were formed by mixing chloroform solutions of the lipids (1 mg/mL), and DSPE PEG2000-biotin (0.1 mol % of final mixture). The mixture was dried with a stream of nitrogen then under vacuum for several hours. The resulting lipid film was hydrated using phosphate buffer saline (PBS) at pH 7.4, which was warmed to a temperature higher than the phase transition temperatures (T_m) of the lipids. After vortex mixing (ca. 10 min) and sonication in a bath sonicator (ca. 5 min), the vesicles solution was used for the formation of SS-BLMs or stored at 4 °C. SS-BLMs were prepared as previously reported,[25] starting with a solution of 5 μm silica beads from Bangs Laboratories (IN, USA), which were washed by centrifugation (10^4 rpm for 10 min) and resuspended at a concentration of 9×10^6 particles/mL in PBS. This solution was coated with avidin (0.1 mg/mL) and washed by centrifugation (3× at 10^4 rpm for 10 min) and resuspension in PBS at the starting volume. The avidin-coated beads were then mixed with an equal volume of lipid SUVs, and vortex mixed for at least 20 min. The resulting lipid-coated beads (i.e., SS-BLMs) were washed by centrifugation (3× at 7×10^3 rpm for 10 min) and resuspension in

DOI: 10.1021/acschemneuro.6b00058
ACS Chem. Neurosci. 2016, 7, 833−841

PBS at the starting volume. Lipid phase separation in SS-BLMs was subsequently induced by the application of two successive heat/cool cycles starting at 4 °C and ending at 80 °C (at a controlled rate of 0.1 °C/s), using a TProfessional Thermocycler (Biometra; Göttingen, Germany).

Cell Culture. Low-density dissociated cell cultures from rat hippocampal neurons were prepared according to a modified protocol described by Banker.[49] Hippocampi were dissected from E17 embryos, treated with 0.25% (w/v) trypsin at 37 °C followed by Dulbecco's modified Eagle's medium (DMEM) supplemented with 10% fetal bovine serum. They were then washed twice Hank's balanced salt solution (HBSS) followed by serum-free Neurobasal medium where they were mechanically dissociated with a glass Pasteur pipet. The dissociated neurons were plated at low density (ca. 1.75×10^4 cm^{-1}) in serum-free Neurobasal medium supplemented with L-glutamine, penicillin, streptomycin, and B-27 on glass coverslips from Ted Pella Inc. previously coated with poly-L-lysine. The cell culture was kept in a humidified 5% CO_2 atmosphere at 37 °C and one-third of the medium was replaced every 3 days. All animal work was performed at the Montreal Neurological Institute in accordance with the Canadian Council of Animal Care Guidelines.

Neurons/SS-BLMs Cocultures. SS-BLMs in sterile PBS solution at pH 7.4 were added dropwise to hippocampal neurons (cultured for at least 14 days in vitro (DIV)) at a concentration of ca. 1.0×10^5 beads/coverslip. After incubation for 24 h in a humidified 5% CO_2 atmosphere at 37 °C, the cells/SS-BLMs cocultures were fixed using 4% (w/v) paraformaldehyde in phosphate buffer at pH 7.4, for 15 min and washed (3× with PBS). Immunofluorescence labeling was achieved by incubating the cells in blocking solution (PBS at pH = 7.4, containing 4% normal donkey serum (NDS) and 0.1% (w/v) saponin) for 30 min, followed by primary antibody solution (1:100 (v/v) rabbit anti-synaptophysin, 1:500 (v/v) mouse anti-bassoon, and/or 1:500 (v/v) rabbit anti-synapsin I in PBS at pH 7.4 containing 0.1% (w/v) saponin and 0.5% (w/v) NDS) overight at 4 °C. After washing (3× in PBS), the cells were incubated in secondary antibody solution (1:500 (v/v) antibodies coupled to Alexa-488, Alexa-543, or Alexa-647 (as appropriate) in PBS at pH 7.4 containing 0.5% (w/v) NDS) for 30 min, then washed (3× in PBS). For F-actin labeling, Alexa-488 or Alexa-647−phalloidin (as appropriate) was used (1:50 (v/v) in the secondary antibody solution). The immunolabeled samples were mounted on microscopic slides using GelTol and sealed prior to imaging.

Confocal Microscopy. Fixed samples were imaged using a LSM-710 confocal microscope (Carl Zeiss AG, Germany) with a 63×/1.4 oil-immersion objective lens. Image fields were first selected using the brightfield (i.e., differential interference contrast, DIC) channel. One (or a combination) of the following optical settings were then applied to acquire the fluorescence images: (i) λ_{ex} 488 nm/λ_{em} LP > 505 nm (single channel imaging) or λ_{em} BP 505−550 nm (multichannel imaging), (ii) λ_{ex} 543 nm/λ_{em} LP > 565 nm, and (iii) λ_{ex} 633 nm/λ_{em} LP > 685 nm. For multichannel imaging, sequential scanning was used. Laser power and detector gain were adjusted to avoid intensity saturation in all acquired images. Z-series image stacks were acquired at a sampling rate which satisfies the Nyquist frequency condition. The acquired image stacks were deconvolved using the blind deconvolution algorithm in AutoQuant X3 software. All images were subject to background subtraction and contrast enhancement (for presentation purposes only) using Imaris 7.4.0 software.

Fluorescence Intensity and Colocalization Quantification. Immunofluorescence and colocalization quantification were calculated using ImageJ 1.49 software for at least 50 beads per experiment and averaged across three separate experiments per condition. Results are presented in histograms which are prepared in KaleidaGraph 4.1 software and display the data mean and standard deviation. The significant difference between experiments is assessed using the two-tailed Student's t test after correction for nonequal variance (see Supporting Information for details and equations of statistical analyses). For intensity quantification, the fluorescence ratio is calculated (using ImageJ 1.49 software) from the average pixel overlap area values within an ROI at the SS-BLM location divided by that of another ROI of exactly the same size and located directly adjacent to the SS-BLM along the neuron (see Supporting Information Figure S3). For analyzing colocalization between synaptic and cytoskeletal proteins with lipid domains, the overlap of their respective fluorescence intensity signals across the surface of the SS-BLM was examined. Colocalization was analyzed quantitatively by calculating the area of overlap between the different fluorescence channels from their respective binary images. Additionally, pixel intensity correlation was performed using the colocalization plugin (Coloc 2) in ImageJ 1.49 software which expressed the Pearson correlation coefficient (PCC) for the colocalization between the fluorescently labeled lipid domains (i.e., S_o domains) and fluorescently labeled proteins.

■ ASSOCIATED CONTENT

Supporting Information

The Supporting Information is available free of charge on the ACS Publications website at DOI: 10.1021/acschemneuro.6b00058.

Details of control experiments, methods used in analyzing fluorescence images, and statistical comparisons (PDF)

■ AUTHOR INFORMATION

Corresponding Authors

*E-mail: bruce.lennox@mcgill.ca.
*E-mail: gopans@icloud.com.

Author Contributions

This project line was initiated by G.G. C.M. designed and performed the experiments as well as the data analysis. C.M. wrote the manuscript with the support of G.G. and R.B.L. All authors have contributed in the results verification and have given approval to the final version of the manuscript.

Funding

This work was funded by the NSERC CREATE Neuroengineering training grant and an NSERC Discovery Grant (RBL).

Notes

The authors declare no competing financial interest.

■ ACKNOWLEDGMENTS

Cell culture work was performed at the McGill Neuro in the laboratory of Prof. Alyson Fournier. Image processing was performed in the Advanced BioImaging Facility of McGill.

■ ABBREVIATIONS

CLSM, confocal laser scanning microscopy; DIV, days in vitro; h, hours; DOPC, 1,2-dioleoyl-*sn*-glycero-3-phosphocholine; DOPE, 1,2-dioleoyl-*sn*-glycero-3-phosphoethanolamine; DOPS, 1,2-dioleoyl-*sn*-glycero-3-phospho-L-serine, sodium salt; DOTAP, 1,2-dioleoyl-3-trimethylammonium-propane, chloride salt; DPPC, 1,2-dipalmitoyl-*sn*-glycero-3-phosphocholine; DPPE, 1,2-dipalmitoyl-*sn*-glycero-3-phosphoethanolamine; DPPS, 1,2-dipalmitoyl-*sn*-glycero-3-phospho-L-serine, sodium salt; DSPE-PEG2000-biotin, 1,2-distearoyl-*sn*-glycero-3-phosphatidylethanolamine-N-biotinyl (polyethylene glycol 2000)], ammonium salt; L_d, liquid disordered phase; N-Rh-DHPE, Lissamine Rhodamine-B-1,2-dihexadecanoyl-*sn*-glycero-phosphoethanolamine, triethylammonium salt; n.s., not significant; PC, phosphatidylcholine; PCC, Pearson correlation coefficient; PDL, poly-D-lysine; PE, phosphatidylethanolamine; PS, phosphatidylserine; ROI, region of interest; S_o, solid-ordered; SS-BLM, spherical supported lipid bilayer membrane

DOI: 10.1021/acschemneuro.6b00058
ACS Chem. Neurosci. 2016, 7, 833−841

REFERENCES

(1) Sebastiao, A. M., Colino-Oliveira, M., Assaife-Lopes, N., Dias, R. B., and Ribeiro, J. A. (2013) Lipid rafts, synaptic transmission and plasticity: impact in age-related neurodegenerative diseases. *Neuropharmacology 64*, 97−107.

(2) Munro, S. (2003) Lipid rafts: Elusive or illusive? *Cell 115*, 377−388.

(3) Lingwood, D., and Simons, K. (2010) Lipid rafts as a membrane-organizing principle. *Science 327*, 46−50.

(4) Golub, T., Wacha, S., and Caroni, P. (2004) Spatial and temporal control of signaling through lipid rafts. *Curr. Opin. Neurobiol. 14*, 542−550.

(5) Kamiguchi, H. (2006) The region-specific activities of lipid rafts during axon growth and guidance. *J. Neurochem. 98*, 330−335.

(6) Michel, V., and Bakovic, M. (2007) Lipid rafts in health and disease. *Biol. Cell. 99*, 129−140.

(7) Paratcha, G., and Ibanez, C. F. (2002) Lipid rafts and the control of neurotrophic factor signaling in the nervous system: variations on a theme. *Curr. Opin. Neurobiol. 12*, 542−549.

(8) Suzuki, T., and Yao, W.-D. (2014) Molecular and structural bases for postsynaptic signal processing: interaction between postsynaptic density and postsynaptic membrane rafts. *J. Neurorestoratol. 2014*, 1−14.

(9) Lindner, R., and Naim, H. Y. (2009) Domains in biological membranes. *Exp. Cell Res. 315*, 2871−2878.

(10) Sonnino, S., and Prinetti, A. (2013) Membrane domains and the "lipid raft" concept. *Curr. Med. Chem. 20*, 4−21.

(11) Simons, K., and Ikonen, E. (1997) Functional rafts in cell membranes. *Nature 387*, 569−572.

(12) Allen, J. A., Halverson-Tamboli, R. A., and Rasenick, M. M. (2007) Lipid raft microdomains and neurotransmitter signalling. *Nat. Rev. Neurosci. 8*, 128−140.

(13) Hering, H., Lin, C. C., and Sheng, M. (2003) Lipid rafts in the maintenance of synapses, dendritic spines, and surface AMPA receptor stability. *J. Neurosci. 23*, 3262−3271.

(14) Simons, K., and Toomre, D. (2000) Lipid rafts and signal transduction. *Nat. Rev. Mol. Cell Biol. 1*, 31−39.

(15) Tillman, T. S., and Cascio, M. (2003) Effects of membrane lipids on ion channel structure and function. *Cell Biochem. Biophys. 38*, 161−190.

(16) Stetzkowski-Marden, F., Recouvreur, M., Camus, G., Cartaud, A., Marchand, S., and Cartaud, J. (2006) Rafts are required for acetylcholine receptor clustering. *J. Mol. Neurosci. 30*, 37−38.

(17) Willmann, R., Pun, S., Stallmach, L., Sadasivam, G., Santos, A. F., Caroni, P., and Fuhrer, C. (2006) Cholesterol and lipid microdomains stabilize the postsynapse at the neuromuscular junction. *EMBO J. 25*, 4050−4060.

(18) Besshoh, S., Chen, S., Brown, I. R., and Gurd, J. W. (2007) Developmental changes in the association of NMDA receptors with lipid rafts. *J. Neurosci. Res. 85*, 1876−1883.

(19) Huang, P., Xu, W., Yoon, S. I., Chen, C. G., Chong, P. L. G., and Liu-Chen, L. Y. (2007) Cholesterol reduction by methyl-beta-cyclodextrin attenuates the delta opioid receptor-mediated signaling in neuronal cells but enhances it in non-neuronal cells. *Biochem. Pharmacol. 73*, 534−549.

(20) Korade, Z., and Kenworthy, A. K. (2008) Lipid rafts, cholesterol, and the brain. *Neuropharmacology 55*, 1265−1273.

(21) Tofoleanu, F., Brooks, B. R., and Buchete, N. V. (2015) Modulation of Alzheimer's Abeta protofilament-membrane interactions by lipid headgroups. *ACS Chem. Neurosci. 6*, 446−455.

(22) Woods, A. S., Colsch, B., Jackson, S. N., Post, J., Baldwin, K., Roux, A., Hoffer, B., Cox, B. M., Hoffer, M., Rubovitch, V., Pick, C. G., Schultz, J. A., and Balaban, C. (2013) Gangliosides and ceramides change in a mouse model of blast induced traumatic brain injury. *ACS Chem. Neurosci. 4*, 594−600.

(23) Sonnino, S., Aureli, M., Mauri, L., Ciampa, M. G., and Prinetti, A. (2015) Membrane lipid domains in the nervous system. *Front. Biosci., Landmark Ed. 20*, 280−302.

(24) Whitehead, S. N., Gangaraju, S., Aylsworth, A., and Hou, S. T. (2012) Membrane raft disruption results in neuritic retraction prior to neuronal death in cortical neurons. *BioSci. Trends 6*, 183−191.

(25) Sebastiao, A. M., Colino-Oliveira, M., Assaife-Lopes, N., Dias, R. B., and Ribeiro, J. A. (2013) Lipid rafts, synaptic transmission and plasticity: impact in age-related neurodegenerative diseases. *Neuropharmacology 64*, 97−107.

(26) Lucido, A. L., Gopalakrishnan, G., Yam, P. T., Colman, D. R., and Lennox, R. B. (2010) Isolation of functional presynaptic complexes from CNS neurons: a cell-free preparation for the study of presynaptic compartments *in vitro*. *ACS Chem. Neurosci. 1*, 535−541.

(27) Lucido, A. L., Suarez-Sanchez, F. S., Thostrup, P., Kwiatkowski, A. V., Leal-Ortiz, S., Gopalakrishnan, G., Liazoghli, D., Belkaid, W., Lennox, R. B., Grutter, P., Garner, C. C., and Colman, D. R. (2009) Rapid assembly of functional presynaptic boutons triggered by adhesive contacts. *J. Neurosci. 29*, 12449−12466.

(28) Gopalakrishnan, G., Thostrup, P., Rouiller, I., Lucido, A. L., Belkaid, W., Colman, D. R., and Lennox, R. B. (2010) Lipid bilayer membrane-triggered presynaptic vesicle assembly. *ACS Chem. Neurosci. 1*, 86−94.

(29) Gopalakrishnan, G., Yam, P. T., Madwar, C., Bostina, M., Rouiller, I., Colman, D. R., and Lennox, R. B. (2011) Label-free visualization of ultrastructural features of artificial synapses *via* cryo-EM. *ACS Chem. Neurosci. 2*, 700−704.

(30) Lai, E. C. (2003) Lipid rafts make for slippery platforms. *J. Cell Biol. 162*, 365−370.

(31) Madwar, C., Gopalakrishnan, G., and Lennox, R. B. (2015) Interfacing living cells and spherically supported bilayer lipid membranes. *Langmuir 31*, 4704−4712.

(32) Baksh, M. M., Dean, C., Pautot, S., DeMaria, S., Isacoff, E., and Groves, J. T. (2005) Neuronal activation by GPI-linked neuroligin-1 displayed in synthetic lipid bilayer membranes. *Langmuir 21*, 10693−10698.

(33) Terrettaz, S., Ulrich, W. P., Guerrini, R., Verdini, A., and Vogel, H. (2001) Immunosensing by a synthetic ligand-gated ion channel. *Angew. Chem., Int. Ed. 40*, 1740−1743.

(34) Bagatolli, L. A., and Gratton, E. (2000) Two photon fluorescence microscopy of coexisting lipid domains in giant unilamellar vesicles of binary phospholipid mixtures. *Biophys. J. 78*, 290−305.

(35) Korlach, J., Schwille, P., Webb, W. W., and Feigenson, G. W. (1999) Characterization of lipid bilayer phases by confocal microscopy and fluorescence correlation spectroscopy. *Proc. Natl. Acad. Sci. U. S. A. 96*, 8461−8466.

(36) Hac, A. E., Seeger, H. M., Fidorra, M., and Heimburg, T. (2005) Diffusion in two-component lipid membranes-a fluorescence correlation spectroscopy and monte carlo simulation study. *Biophys. J. 88*, 317−333.

(37) Bewick, V., Cheek, L., and Ball, J. (2003) Statistics review 7: correlation and regression. *Crit. Care. 7*, 451−459.

(38) Ziv, N. E., and Garner, C. C. (2004) Cellular and molecular mechanisms of presynaptic assembly. *Nat. Rev. Neurosci. 5*, 385−399.

(39) MacGillavry, H. D., Kerr, J. M., and Blanpied, T. A. (2011) Lateral organization of the postsynaptic density. *Mol. Cell. Neurosci. 48*, 321−331.

(40) Israelachvili, J. N., Marcelja, S., and Horn, R. G. (1980) Physical principles of membrane organization. *Q. Rev. Biophys. 13*, 121−200.

(41) Vance, J. E., and Tasseva, G. (2013) Formation and function of phosphatidylserine and phosphatidylethanolamine in mammalian cells. *Biochim. Biophys. Acta, Mol. Cell Biol. Lipids 1831*, 543−554.

(42) Wen, Z., and Zheng, J. Q. (2006) Directional guidance of nerve growth cones. *Curr. Opin. Neurobiol. 16*, 52−58.

(43) Tuft, B. W., Zhang, L., Xu, L., Hangartner, A., Leigh, B., Hansen, M. R., and Guymon, C. A. (2014) Material stiffness effects on neurite alignment to photopolymerized micropatterns. *Biomacromolecules 15*, 3717−3727.

(44) Gupta, M., Sarangi, B. R., Deschamps, J., Nematbakhsh, Y., Callan-Jones, A., Margadant, F., Mege, R. M., Lim, C. T., Voituriez, R.,

DOI: 10.1021/acschemneuro.6b00058
ACS Chem. Neurosci. 2016, 7, 833−841

and Ladoux, B. (2015) Adaptive rheology and ordering of cell cytoskeleton govern matrix rigidity sensing. *Nat. Commun. 6*, 7525.
(45) Daly, W., Yao, L., Zeugolis, D., Windebank, A., and Pandit, A. (2012) A biomaterials approach to peripheral nerve regeneration: bridging the peripheral nerve gap and enhancing functional recovery. *J. R. Soc., Interface 9*, 202−221.
(46) Tyler, W. J. (2012) The mechanobiology of brain function. *Nat. Rev. Neurosci. 13*, 867−878.
(47) Doherty, G. J., and McMahon, H. T. (2008) Mediation, modulation, and consequences of membrane-cytoskeleton interactions. *Annu. Rev. Biophys. 37*, 65−95.
(48) Janmey, P. A. (1998) The cytoskeleton and cell signaling: component localization and mechanical coupling. *Physiol. Rev. 78*, 763−781.
(49) Goslin, K., Asmussen, H., and Banker, G. In *Culturing Nerve Cells*. Banker, G., and Golin, K., Eds.; 2nd ed.; MIT Press: Cambridge, Massachusetts, 1998, p. 666.

DOI: 10.1021/acschemneuro.6b00058
ACS Chem. Neurosci. 2016, 7, 833−841